Springer

Journal of
Mechanical
Science and
Technology

Journal of Mechanical Science and Technology 22 (2008) 835~845

www.springerlink.com/content/1738-494x

Stress analysis of two-dimensional cellular materials with thick cell struts

Dohyung Lim[1], Han Sung Kim[1,*], Young Ho Kim[1], Yoon Hyuk Kim[2] and S.T.S. Al-Hassani[3]

[1]*Department of Biomedical Engineering and Research Institute for Medical Instruments & Rehabilitation Engineering, Yonsei University, Wonju, Kangwon, Republic of Korea*

[2]*School of Advanced Technology, Research Institute of Biomechanical Engineering, Kyunghee University, Yongin, Kyunggi, Republic of Korea*

[3]*Department of Mechanical, Aerospace & Manufacturing Engineering, University of Manchester, Manchester, United Kingdom*

(Manuscript Received March 13, 2007; Revised December 17, 2007; Accepted February 4, 2008)

Abstract

Finite element analyses (FEA) were performed to thoroughly validate the collapse criteria of cellular materials presented in our previous companion paper. The maximum stress (von-Mises stress) on the cell strut surface and the plastic collapse stress were computed for two-dimensional (2D) cellular materials with thick cell struts. The results from the FEA were compared with those from theoretical criteria of authors. The FEA results were in good agreement with the theoretical results. The results indicate that when bending moment, axial and shear forces are considered, the maximum stress on the strut surface gives significantly different values in the tensile and compressive parts of the cell wall as well as in the two loading directions. Therefore, for the initial yielding of ductile cellular materials and the fracture of brittle cellular materials, in which the maximum stress on the strut surface is evaluated, it is necessary to consider not only the bending moment but also axial and shear forces. In addition, this study shows that for regular cellular materials with the identical strut geometry for all struts, the initial yielding and the plastic collapse under a biaxial state of stress occur not only in the inclined cell struts but also in the vertical struts. These FEA results support the theoretical conclusion of our previous companion paper that the anisotropic 2D cellular material has a truncated yield surface not only on the compressive quadrant but also on the tensile quadrant.

Keywords: Cellular materials; Thick cell struts; Collapse criteria; von-Mises stress; Truncated yield surface

1. Introduction

In practice, we often encounter cellular materials which have a network of doubly tapered struts in their microstructures, such as trabecular bones. However, in order to analyze the strength of cellular materials, past investigators [1-5] used simple beam theories which are only valid for cellular structures composed of uniform struts. Recently, many researchers have used computer models with multiple cells, and included various imperfections and irregularities [6-16]. Kim and Al-Hassani [17, 18] proposed the plastic collapse criteria for cellular materials composed of doubly tapered struts have been analyzed under uniaxial and biaxial loading conditions. They [17, 18] analyzed the effect of doubly tapered strut morphology on the plastic yield surface of cellular materials. Their results [17, 18] indicated that the anisotropic honeycomb of Gibson and Ashby [5] has a truncated yield surface not only on the compressive quadrant but also on the tensile quadrant.

One of main aims of this study is to validate the collapse criteria developed by Kim and Al-Hassani [17, 18] by using the finite element method. The results from the FEA are compared with those from their theoretical criteria. In addition, the maximum stress (von-Mises stress) on the strut surface of cellu-

*Corresponding author. Tel.: +82 33 760 2342, Fax.: +82 33 760 2913
E-mail address: hanskim@yonsei.ac.kr
DOI 10.1007/s12206-008-0202-6

lar materials is analyzed and compared with the results from the FEA.

2. Analysis

2.1 In-plane plastic collapse stress of hexagonal cellular materials

In the present study, the results of Kim and Al-Hassani [17, 18] are extended to those for the maximum stress on the strut surface.

In the hexagonal cellular structure as shown in Fig. 1 [18], the overall yield surface for this structure has been shown to consist of intersection surfaces of particular collapse modes. Under an in-plane biaxial stress state, collapse modes are characterized as 'Mode ℓ,' 'Mode h' and 'Mode ℓ_ex', depending on which parts of struts fail, as described by Kim and Al-Hassani [17, 18]. When the action of two principal tensile stresses coincides with the axes of symmetry of the structure, characteristic plastic collapse modes for the hexagonal cellular structure with a rectangular cross-section in its strut are given in Table 1. Upon substitution for $Z_\lambda = bt(x_\lambda)^2/4$, $A_\lambda = bt(x_\lambda)$, $\ell_v = b$ and $A_0 = A_{h0} = bt_0$, the equations given in Table 1 reduce to those for honeycombs composed of doubly tapered struts.

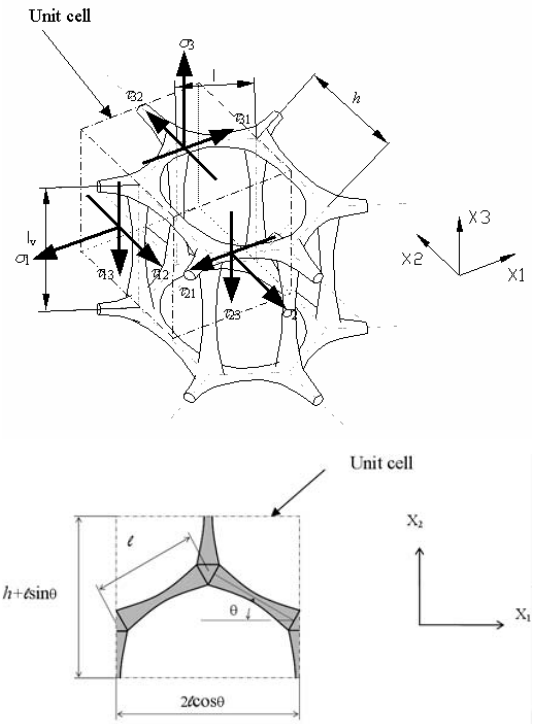

Fig. 1. Hexagonal model of rod-like columnar structure and unit cell.

Table 1. In-plane plastic collapse stress for general hexagonal columnar structures [9, 10].

Mode	Plastic collapse stress	Axial stress
Mode l (Uniaxial)	$\frac{\sigma_1}{\sigma_{ys}} = \frac{2Z_\lambda}{\lambda\ell\ell_v(h/\ell+\sin\theta)\sin\theta}\left[1-\left\{\frac{\sigma_a}{\sigma_{ys}}\right\}^2\right]$	$\sigma_a = \frac{\sigma_1\ell\ell_v(h/\ell+\sin\theta)\cos\theta}{A_\lambda}$
	$\frac{\sigma_2}{\sigma_{ys}} = \frac{Z_\lambda}{\lambda\ell}\frac{2}{\ell_v\cos^2\theta}\left[1-\left\{\frac{\sigma_a}{\sigma_{ys}}\right\}^2\right]$	$\sigma_a = \frac{\sigma_2\ell\ell_v\sin\theta\cos\theta}{A_\lambda}$
	$\frac{\tau_{12}}{\sigma_{ys}} = \frac{Z_\lambda}{\ell\lambda}\frac{2}{(h/\ell)\ell_v\cos\theta}\left[1-\left\{\frac{\sigma_a}{\sigma_{ys}}\right\}^2\right]$	$\sigma_a = \frac{\tau_{12}\ell\ell_v\{1+(h/\ell)\sin\theta\}}{A_\lambda}$
Mode h (Uniaxial)	$\frac{\sigma_2}{\sigma_{ys}} = \frac{A_{h0}}{2\ell\ell_v\cos\theta}$	
	$\frac{\tau_{12}}{\sigma_{ys}} = \frac{Z_{\lambda h}}{\ell^2}\frac{1}{(\lambda_h/\ell)\ell_v\cos\theta}$	
Mode l_ex (Biaxial)	$\frac{\sigma_1}{\sigma_{ys}} = \frac{A_0}{\ell\ell_v(\cot\theta+\tan\theta)(h/\ell+\sin\theta)\sin\theta}$	
	$\frac{\sigma_2}{\sigma_{ys}} = \frac{A_0}{\ell\ell_v(\cot\theta+\tan\theta)\cos^2\theta}$	
Mode h (Biaxial)	$\frac{\sigma_2}{\sigma_{ys}} = \frac{A_{h0}}{2\ell\ell_v\cos\theta}$	

2.2 Stresses on the strut surface of cellular materials

In a uniform strut the maximum normal stresses always occur at a cross section of maximum bending moment. This is because the stress varies along the axis of the beam in the same manner as the bending moment. However, this conclusion does not necessary apply to non-uniform struts, because for such beams the stress varies along the strut axis not only in proportion to the bending moment but also in inverse proportion to the second moment of area of the cross-section. In addition, the distribution of shear stresses in a non-uniform strut is quite different from that in a uniform strut. Gere and Timoshenko [19] derived an approximate expression for the shear stress that incorporated the effect of changing cross section of the strut. They described that if the cross-sectional dimensions change gradually along the strut length, normal and shear stresses can be calculated, with good accuracy, respectively, from the flexure formula and the approximate expression for the shear stress presented by them. Thus, their approximate equations are used in this study.

2.2.1 Normal stress on a non-uniform strut

In the hexagonal cellular structure as shown in Fig. 2 [18], the remote stress σ_1 in the X_1 direction produces stress resultants in the form of axial forces ($R = P\cos\theta$), shear forces ($V = P\sin\theta$) and bending moments ($M = Vx$) on the in-plane ℓ struts. For elastic deformations, the state of stress associated with each of these stress resultants is linearly related to the strain, so the principal of superposition is applicable. Thus, for a cross section at distance x from the mid-span of the struts, the total normal stress σ_x acting on the strut surface is the sum of contributions from the individual stress resultants as follows:

$$\sigma_x = \frac{Vx}{S(x)} + \frac{R}{A(x)} \tag{1}$$

where $S(x)$ is the section modulus of the cross-sectional area $A(x)$, R is positive when it produces tension, and Vx is positive according the bending-moment sign convention.

From Fig. 2, we have $P = \sigma_1(h + \ell\sin\theta)\ell_v$, which makes equation (1)

$$\frac{\sigma_x}{\sigma_1} = \frac{[\ell\ell_v(h/\ell + \sin\theta)\sin\theta]x}{S(x)} + \frac{\ell\ell_v(h/\ell + \sin\theta)\cos\theta}{A(x)} \tag{2}$$

.

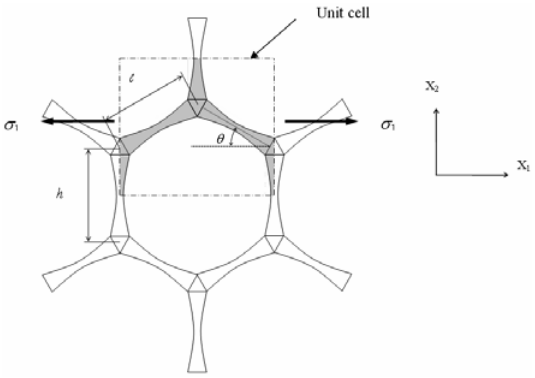

(a)

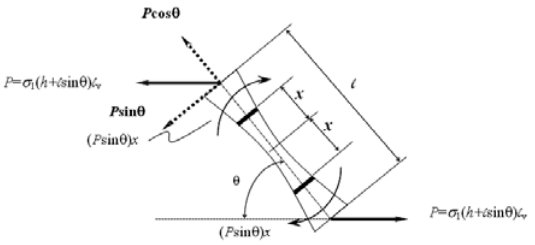

(b)

Fig. 2. Forces and moments on the ℓ strut due to the uniaxial stress in the X_1 direction: (a) the unit cell; (b) Mode ℓ.

Table 2. Normal and shear stresses on the strut surface of hexagonal columnar structures.

Mode		$\sigma_x = \frac{Vx}{S(x)} + \frac{R}{A(x)}$, $\tau_{xy} = \frac{Vxt(x)}{4I(x)}\frac{dt(x)}{dx}$
Mode *l* (Uniaxial)	σ_1	$V = \sigma_1\ell\ell_v(h/\ell + \sin\theta)\sin\theta$ $R = \sigma_1\ell\ell_v(h/\ell + \sin\theta)\cos\theta$
	σ_2	$V = \sigma_2\ell\ell_v\cos^2\theta$ $R = \sigma_2\ell\ell_v\sin\theta\cos\theta$
	τ_{12}	$V = \tau_{12}h\ell_v\cos\theta$ $R = \tau_{12}\ell\ell_v[1 + (h/\ell)\sin\theta]$
Mode *h* (Uniaxial)	σ_2	$V = 0$ $R = 2\sigma_2\ell\ell_v\cos\theta$
	τ_{12}	$V = 2\tau_{12}\ell\ell_v\cos\theta$ $R = 0$
Mode *l_ex* (Biaxial)	σ_1	$V = 0$ $R = \sigma_1\ell\ell_v(\cot\theta + \tan\theta)(h/\ell + \sin\theta)\sin\theta$
	σ_2	$V = 0$ $R = \sigma_2\ell\ell_v(\cot\theta + \tan\theta)\cos^2\theta$
Mode *h* (Biaxial)	σ_2	$V = 0$ $R = 2\sigma_2\ell\ell_v\cos\theta$

The summary of axial forces R, shear forces V and bending moments Vx for other collapse modes is given in Table 2.

2.2.2 Shear stress on a non-uniform strut

In the case of a strut of rectangular cross section ($I(x) = bt(x)^3/12$) with constant width b and varying thickness $t(x)$, shear stress τ_{xy} in a non-uniform strut is given as [19]:

$$\tau_{xy} = \frac{VQ_1}{I(x)b} + \frac{Mt(x)}{4I(x)}\left(1 - \frac{Q_1 t(x)}{I(x)}\right)\frac{dt(x)}{dx} \tag{3}$$

where Q_1 is the first moment of the cross-sectional area of the strut above the level y_1 at which the shear stress acts and $Q_1 = b/2(h^2/4 - y_1^2)$ for rectangular cross section.

The shear stress τ_{xy} at any cross section is dependent not only upon the shear force V but also upon the bending moment $M = Vx$ and the rate of change of $t(x)$ with respect to x.

When $Q_1 = 0$ (at the top and bottom surfaces of the strut), equation (3) reduces to:

$$\tau_{xy} = \frac{Vxt(x)}{4I(x)}\frac{dt(x)}{dx} \tag{4}$$

which shows that unlike the case of uniform struts the shear stress on the outer surfaces of non-uniform struts is not zero, except that it is zero at the mid-span of the strut. Therefore, we incorporate both normal and shear stresses in the combined stress resultant on the outer surfaces of non-uniform struts.

The expressions for shear force V for other collapse modes are summarized in Table 2. Upon substitution for $I(x) = bt(x)^3/12$, $S(x) = bt(x)^2/6$, $A(x) = bt(x)$, $A_0 = A_{h0} = bt_0$ and $\ell_v = b$, equations given in Table 2 reduce to those for the 2D cellular material. In the present study, the strut material is assumed to satisfy the von-Mises yield criterion with uniaxial yield stress σ_{ys}. Thus, the von-Mises stress σ_e on the external surfaces of a non-uniform strut for this combined state of stress becomes:

$$\sigma_e = \sqrt{\sigma_x^2 + 3\tau_{xy}^2}\ . \tag{5}$$

Taking the derivative $d\sigma_e/dx$ and equating it to zero gives the location where σ_e is a maximum.

2.3 Finite element methodology

Kim and Al-Hassani [20] predicted the effective elastic constants of 2D cellular materials with thick cell walls by using modified unit cell approaches. In the present study, the loading and boundary schemes described by Kim and Al-Hassani [20] are extended to those under a biaxial loading condition as shown in Table 3. The schemes under uniaxial loading condition are similar to those of the compliance matrix method for the effective elastic constants described by Kim and Al-Hassani [20]. Fig. 3 shows the loading and boundary schemes under biaxial loading condition, used in the ABAQUS input data file, to evaluate the maximum stress on the strut surface and the plastic collapse stress of 2D cellular materials with thick cell struts. Auxiliary nodes (Node1, Node2, Node3, Node4) used for defining applied load and boundary conditions are also shown in Fig. 3. The auxiliary nodes associated with each face were constrained with the nodes on that face. Two faces of the unit cell were fixed in the X_1 and X_2 directions, respectively, to prevent rigid body movement. Two unconstrained faces were subjected, through the associated auxiliary nodes, to the in-plane loads that were generated in each face. The schemes under uniaxial and biaxial loading conditions are summarized in Table 3. From these schemes, the maximum stress on the strut surface and the plastic collapse stress can be computed directly and easily.

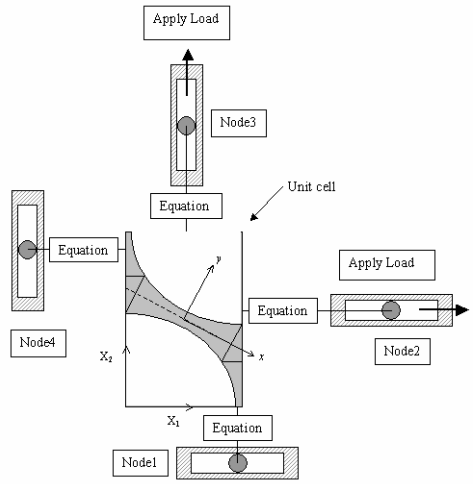

Fig. 3. Unit cell of a typical hexagonal honeycomb with tapered strut morphology, showing the applied loading and boundary conditions to evaluate the maximum stress on the strut surface and the plastic collapse stress under biaxial loading condition.

Table 3. The loads and boundary conditions (for the compliance matrix method) applied to the faces via the associated auxiliary nodes of the unit cell used to calculate the maximum stress on the strut and the plastic collapse stress.

Stress factors	Loading direction and boundary conditions				
	Node1	Node2	Node3	Node4	Loading Mode
σ_e/σ_1, $(\sigma^*_{pl})_1/\sigma_{ys}$	YFIX(1)	XCLOAD(2)	FREE	XFIX	Direct (Uniaxial)
σ_e/σ_2, $(\sigma^*_{pl})_2/\sigma_{ys}$	YFIX	FREE	YCLOAD	XFIX	Direct (Uniaxial)
σ_e/τ_{12}, $(\tau^*_{pl})_{12}/\sigma_{ys}$	XFIX(1)	YCLOAD(2)	XCLOAD	YFIX	Shear (Uniaxial)
σ_e/σ_1, σ_e/σ_2 σ_1/σ_{ys}, σ_2/σ_{ys}	YFIX	XCLOAD	YCLOAD	XFIX	Direct (Biaxial)

(1): XFIX and YFIX indicate fixity in the X_1 and X_2 directions.
(2): XCLOAD and YCLOAD indicate the application of a concentrated point load equivalent to unit nominal stress on the unit cell in X_1 and X_2 directions, respectively.

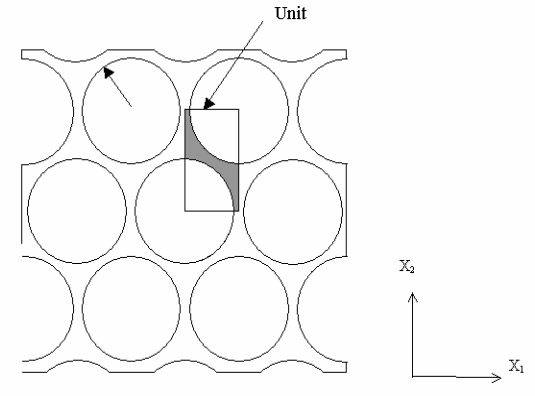

(a) Plan view

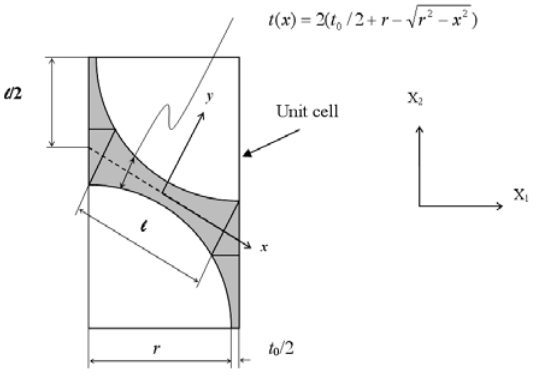

(b) Geometry of unit cell

Fig. 4. Typical cellular material with thick cell struts: (a) plan view; (b) geometry of unit cell.

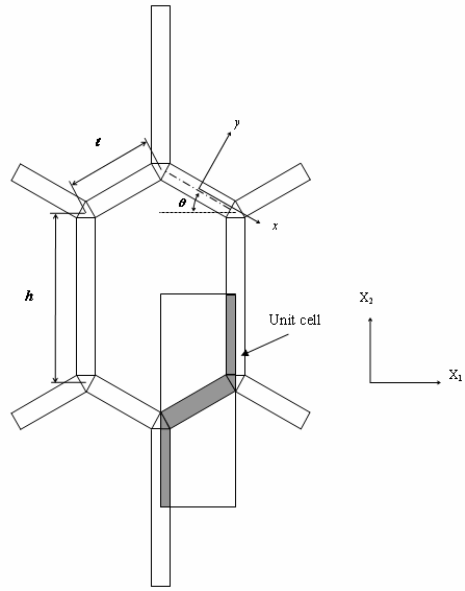

Fig. 5. Plan view of an anisotropic cellular material ($h/\ell = 2$, $\theta = 45°$ and $t/\ell = 0.1$).

3. Results

The standard (implicit) version of the ABAQUS FE code was used to compute the maximum stress (von-Mises stress) on the strut surface and the plastic collapse stress for 2D cellular materials with thick cell struts. Plan views of 2D cellular materials analyzed in this study are shown in Figs. 4 [21] and 5. The FE analysis provides results that are in good agreement with the theoretical results.

3.1 Regular cellular material with doubly tapered struts

At large relative densities above about 0.3 (30%), the material is better thought of as a solid with holes in it, not as a cellular material [5]. This study was concerned with the true cellular materials, and thus with relative densities of less than 0.30. Therefore, as an example of regular cellular materials with doubly tapered struts, perforated plates with relative densities of 0.1815 and 0.2654 were analyzed for this study. The maximum stress (von-Mises stress) on the strut surface and the plastic collapse stress for the cellular materials were analyzed under uniaxial and biaxial load schemes given in Table 3. The results from the FE analysis are compared with those of theoretical equations (Tables 1 and 2) in Tables 4-7, in which ρ_M^* represents the relative density of these 2D cellular materials.

Tables 4 and 5 show that under uniaxial loading, bending is the dominant mode for the maximum stress on the strut surface, but axial and shear loads are also important modes to be considered. When bending moment, axial and shear forces are considered, σ_e/σ_1 and σ_e/σ_2 provide significantly different values in tension and compression parts of the strut as well as in the X_1 and X_2 directions. These results are in a good agreement with the results of FEA. However, for the plastic collapse stress under uniaxial loading, the bending moment is highly dominant and the contribution of the axial load is small compared with that from the bending moment as shown in Tables 6 and 7.

Under biaxial loads, 'Mode ℓ_*ex*' and 'Mode *h*' may occur at the same time because both modes have the same stress value as shown in Tables 4~7. Figs. 6 and 7 show contour plots for the stress factors of the regular honeycombs with doubly tapered struts under uniaxial and biaxial loadings.

Table 4. Maximum stress on the strut surface (von Mises stress) for the regular hexagonal honeycomb with tapered strut morphology, normalized with regard to applied stress ($\rho_M^* = 0.1815$, $E = 2\times10^5$ Nmm^{-2}, $\nu = 0.3$ and $G = 0.7692\times10^5$Nmm^{-2}).

Stress factors		Stress analysis condition			
		ABAQUS (plane stress)	Bending	Bending+Axial	Bending+Axial +Shear
σ_e/σ_1 (Uniaxial)	Mode *l* (tension part)	65.7 (1.82)	51.8 (1.76)	63.3 (1.64)	65.3 (1.74)
	Mode *l* (compression part)	42.6 (-2.03)	51.8 (-1.76)	40.7 (-1.90)	44.9 (-2.08)
σ_e/σ_2 (Uniaxial)	Mode *l* (tension part)	57.8 (-1.90)	51.8 (-1.76)	55.6 (-1.72)	58.1 (-1.84)
	Mode *l* (compression part)	50.1 (1.95)	51.8 (1.76)	48.0 (1.80)	51.3 (1.95)
σ_e/τ_{12} (Uniaxial)	Mode *h* (tension part)	125.5 (1.86)	119.6 (1.76)	119.6 (1.76)	126.3 (1.89)
	Mode *h* (compression part)	125.5 (1.86)	119.6 (-1.76)	119.6 (-1.76)	126.3 (-1.89)
σ_e/σ_1 (Biaxial)	Mode *l_ex* Mode *h*	20.7 (0.0)	-	20.0 (0.0)	20.0 (0.0)
σ_e/σ_2 (Biaxial)	Mode *l_ex* Mode *h*	20.7 (0.0)	-	20.0 (0.0)	20.0 (0.0)

The values in parentheses are those of *x* for which each stress factor is a maximum.

Table 5. Maximum stress on the strut surface (von Mises stress) for the regular hexagonal honeycomb with tapered strut morphology, normalized with regard to applied stress ($\rho_M^* = 0.2654$, E = 2×10^5Nmm^{-2}, ν = 0.3 and G = 0.7692×10^5 Nmm^{-2}).

Stress factors		Stress analysis condition			
		ABAQUS (plane stress)	Bending	Bending+Axial	Bending+Axial +Shear
σ_e / σ_1 (Uniaxial)	Mode *l* (tension part)	26.0 (2.46)	17.7 (2.40)	23.5 (2.17)	24.9 (1.74)
	Mode *l* (compression part)	14.2 (-3.08)	17.7 (-2.40)	12.2 (-2.67)	16.0 (-3.28)
σ_e / σ_2 (Uniaxial)	Mode *l* (tension part)	22.0 (-2.68)	17.7 (-2.40)	19.6 (-2.32)	21.5 (-2.67)
	Mode *l* (compression part)	18.0 (2.99)	17.7 (2.40)	15.9 (2.48)	18.5 (2.95)
σ_e / τ_{12} (Uniaxial)	Mode *h* (tension part)	46.2 (2.89)	41.0 (2.40)	41.0 (2.40)	46.1 (2.80)
	Mode *h* (compression part)	46.2 (2.89)	41.0 (-2.40)	41.0 (-2.40)	46.1 (-2.80)
σ_e / σ_1 (Biaxial)	Mode *l_ex* Mode *h*	10.7 (0.0)	-	10.0 (0.0)	10.0 (0.0)
σ_e / σ_2 (Biaxial)	Mode *l_ex* Mode *h*	10.7 (0.0)	-	10.0 (0.0)	10.0 (0.0)

The values in parentheses are those of x for which each stress factor is a maximum.

Table 6. Plastic collapse stress for the regular hexagonal honeycombs with tapered strut morphology, normalized with regard to material yield stress ($\rho_M^* = 0.1815$).

Stress factors		Stress analysis condition		
		ABAQUS (plane stress)	Bending	Bend-ing+Axial
$(\sigma_{pl}^*)_1 / \sigma_{ys}$ (Uniaxial)	Mode *l*	0.0264 (1.69)	0.0290 (1.76)	0.0263 (1.65)
$(\sigma_{pl}^*)_2 / \sigma_{ys}$ (Uniaxial)	Mode *l*	0.0287 (-1.76)	0.0290 (-1.76)	0.0286 (-1.75)
$(\tau_{pl}^*)_{12} / \sigma_{ys}$ (Uniaxial)	Mode *h*	0.0125 (1.80)	0.0125 (1.76)	0.0125 (1.76)
σ_1 / σ_{ys} (Biaxial)	Mode *l_ex* Mode *h*	0.0509	-	0.0500 (0.0)
σ_2 / σ_{ys} (Biaxial)	Mode *l_ex* Mode *h*	0.0509	-	0.0500 (0.0)

The values in parentheses are those of x for which each stress factor is a maximum.
(σ_{ys} = 1Nmm^{-2}, E = 2×10^5Nmm^{-2}, ν = 0.3 and G = 0.7692×10^5Nmm^{-2}).

Table 7. Plastic collapse stress for the regular hexagonal honeycombs with tapered strut morphology, normalized with regard to material yield stress ($\rho_M^* = 0.2654$).

Stress factors		Stress analysis condition		
		ABAQUS (plane stress)	Bending	Bend-ing+Axial
$(\sigma_{pl}^*)_1 / \sigma_{ys}$ (Uniaxial)	Mode *l*	0.0689 (2.074)	0.0846 (2.397)	0.0704 (2.1215)
$(\sigma_{pl}^*)_2 / \sigma_{ys}$ (Uniaxial)	Mode *l*	0.0794 (2.592)	0.0846 (-2.397)	0.0825 (-2.363)
$(\tau_{pl}^*)_{12} / \sigma_{ys}$ (Uniaxial)	Mode *h*	0.0353 (2.375)	0.0366 (2.397)	0.0366 (2.397)
σ_1 / σ_{ys} (Biaxial)	Mode *l_ex* Mode *h*	0.1029 (0.0)	-	0.1000 (0.0)
σ_2 / σ_{ys} (Biaxial)	Mode *l_ex* Mode *h*	0.1029 (0.0)	-	0.1000 (0.0)

The values in parentheses are those of x for which each stress factor is a maximum.
(σ_{ys} = 1Nmm^{-2}, E = 2×10^5Nmm^{-2}, ν = 0.3 and G = 0.7692×10^5Nmm^{-2}).

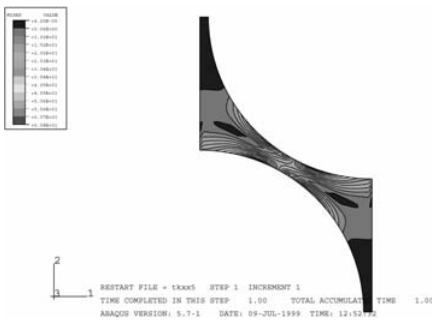

(a) σ_e / σ_1 (Mode ℓ under uniaxial loading)

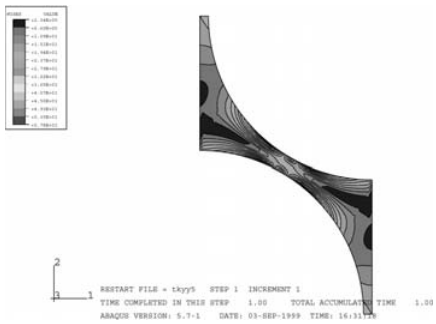

(b) σ_e / σ_2 (Mode ℓ under uniaxial loading)

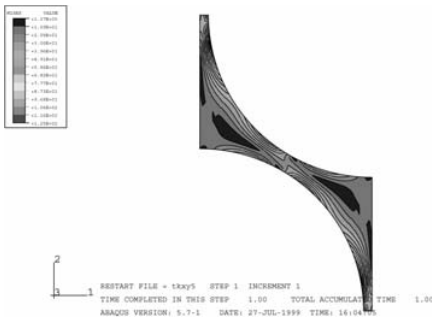

(c) σ_e / τ_{12} (Mode h under uniaxial loading)

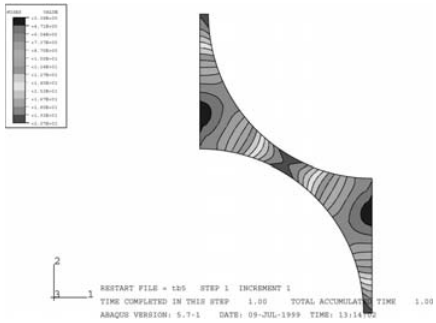

(d) σ_e / σ_1, σ_e / σ_2 (Mode ℓ_ex, Mode h under biaxial loading)

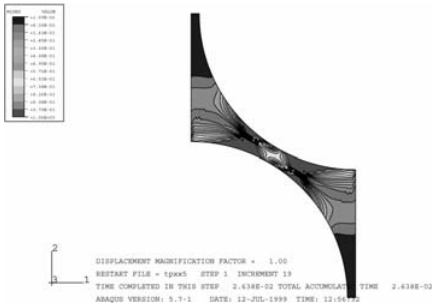

(e) $(\sigma^*_{pl})_1 / \sigma_{ys}$ (Mode ℓ under uniaxial loading)

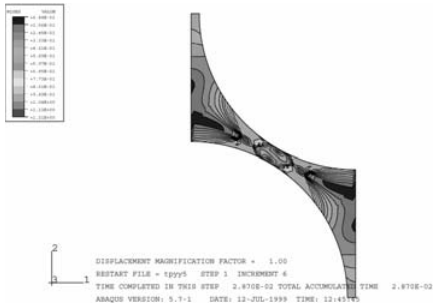

(f) $(\sigma^*_{pl})_2 / \sigma_{ys}$ (Mode ℓ under uniaxial loading)

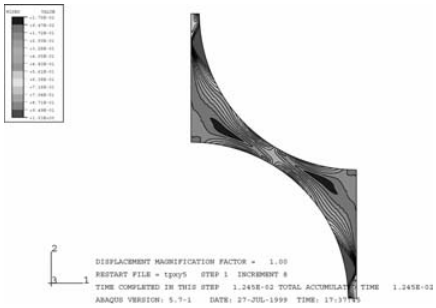

(g) $(\tau^*_{pl})_{12} / \sigma_{ys}$ (Mode h under uniaxial loading)

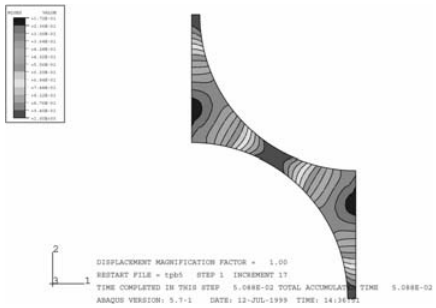

(h) σ_1 / σ_{ys}, σ_2 / σ_{ys} (Mode ℓ_ex, Mode h under biaxial loading)

Fig. 6. (a) to (h) Contour plots for the stress factors of the regular cellular material with doubly tapered struts ($\rho^*_M = 0.1815$).

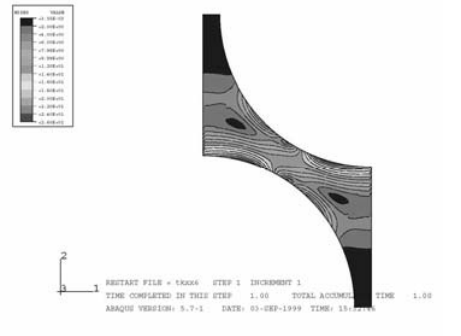

(a) σ_e / σ_1 (Mode ℓ under uniaxial loading)

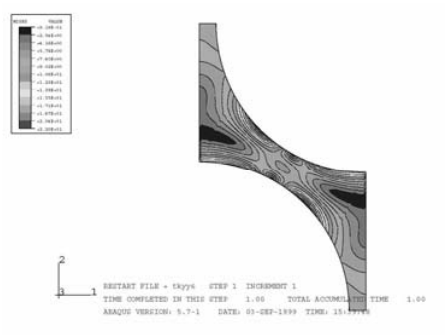

(b) σ_e / σ_2 (Mode ℓ under uniaxial loading)

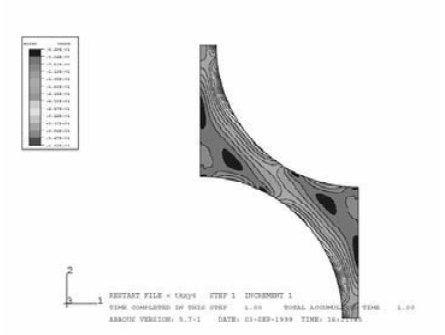

(c) σ_e / τ_{12} (Mode *h* under uniaxial loading)

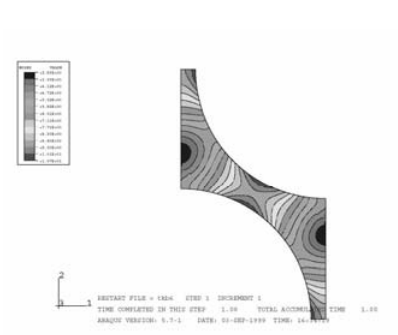

(d) σ_e / σ_1, σ_e / σ_2 (Mode ℓ_*ex*, Mode *h* under biaxial loading)

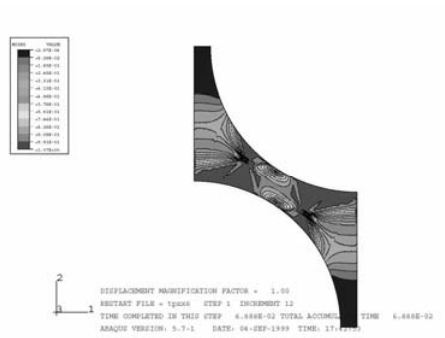

(e) $(\sigma^*_{pl})_1 / \sigma_{ys}$ (Mode ℓ under uniaxial loading)

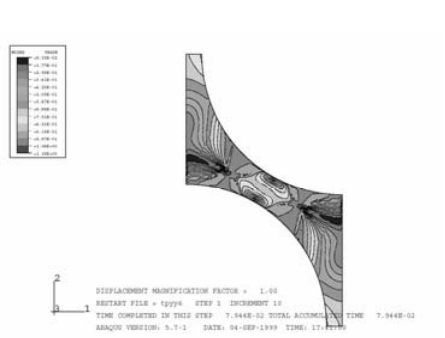

(f) $(\sigma^*_{pl})_2 / \sigma_{ys}$ (Mode ℓ under uniaxial loading)

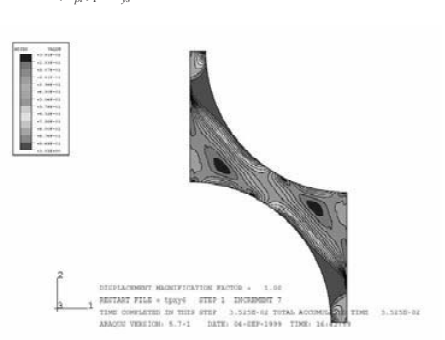

(g) $(\tau^*_{pl})_{12} / \sigma_{ys}$ (Mode *h* under uniaxial loading)

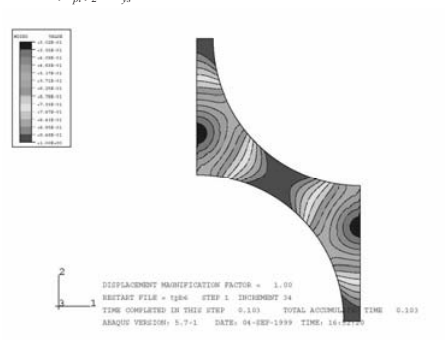

(h) σ_1 / σ_{ys}, σ_2 / σ_{ys} (Mode ℓ_*ex*, Mode *h* under biaxial loading)

Fig. 7. (a) to (h) Contour plots for the stress factors of the regular cellular material with doubly tapered struts ($\rho^*_M = 0.2654$).

3.2 Anisotropic honeycomb with uniform struts

Fig. 5 shows the unit cell model for an anisotropic honeycomb ($h/l = 2$, $\theta = 45°$ and $t/l = 0.1$) of Gibson and Ashby [5]. They described that the plastic yield surface is truncated only on the compressive side by the elastic buckling failure surface.

In the present study, the plastic collapse stress for the anisotropic honeycomb was analyzed under biaxial load schemes given in Table 3. As a result, the plastic yield stress due to the collapse 'Mode *h*' is $\sigma_2 = 0.071\sigma_{ys}$, which is the same as that analyzed by Kim and Al-Hassani [18]. This result supports the theoretical conclusion of Kim and Al-Hassani [18] that the anisotropic honeycomb of Gibson and Ashby [5] has a truncated yield surface not only on the compressive quadrant but also on the tensile quadrant. Thus, this anisotropic honeycomb has no extreme point ('Mode ℓ_*ex*') at which the two yield surfaces intersect in the tensile quadrant. Fig. 8 shows the contour plot for the plastic collapse 'Mode *h*' under a biaxial loading condition.

4. Discussion and conclusions

The FE analysis presented here using the implicit version of the ABAQUS code generates results that are in excellent agreement with those from theory. The results from the FE analysis also favorably support collapse criteria developed by Kim and Al-Hassani [17, 18]. The fundamental advantage of the technique employed here is that it is relatively easy to use and is independent of the type of cellular material. Once a unit cell of a cellular material is identified, the analysis can be implemented in the same manner as outlined in this study.

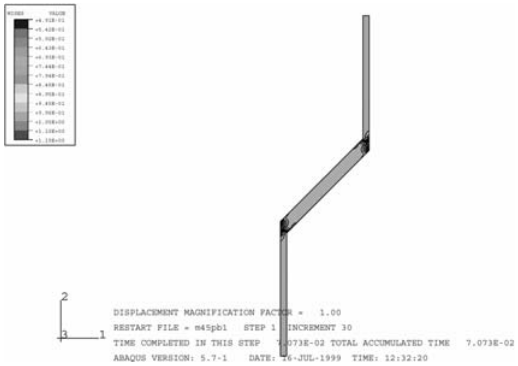

Fig. 8. Contour plot for the plastic collapse stress (Mode *h*) of an anisotropic cellular material ($h/\ell = 2$, $\theta = 45°$ and $t/\ell = 0.1$) under biaxial loading condition.

The results indicate that when axial and shear forces are neglected, a regular hexagon has the same uniaxial stress value in the X_1 and X_2 directions, as Gibson and Ashby [5] mentioned. However, when bending moment, axial and shear forces are considered, the maximum stress on the strut surface gives significantly different values in the tensile and compressive parts of the strut as well as in the X_1 and X_2 directions. Thus, for the initial yielding of ductile cellular materials and the fracture of brittle cellular materials, in which the maximum stress on the strut surface is evaluated, it is necessary to consider not only bending moment but also axial and shear forces.

In the case of the plastic collapse stress, the bending moment is highly dominant. The contribution of the axial load to the plastic collapse stress under uniaxial loading is small compared with that from the bending moment, although in the biaxial case it can be the dominant contribution to the plastic collapse.

It is also found that if the strut material of cellular materials has the same tensile and compressive strengths, the initial yield occurs in the tensile part of the strut surface for uniaxial tensile loading, while it does in the compressive part of the strut surface for uniaxial compressive loading. In addition, this study shows that for regular cellular materials with the identical strut geometry for all struts, the initial yielding and the plastic collapse under a biaxial state of stress occur not only in the inclined cell struts but also in the vertical struts.

The results of the FEA support the theoretical conclusion of Kim and Al-Hassani [18] that the anisotropic 2D cellular material of Gibson and Ashby [5] has a truncated yield surface not only on the compressive quadrant but also on the tensile quadrant.

Acknowledgments

This research was supported by the Program for the Training of Graduate Students in Regional Innovation which was conducted by the Ministry of Commerce Industry and Energy of the Korean Government. Additionally, the authors wish to thank Prof. W. J. Stronge (University of Cambridge) and Dr. S. Li (University of Manchester) for their useful comments on the original work upon which this paper is based.

Nomenclature

$A(x)$: Area function of cell walls
b : Cell wall depth of cellular materials

E^* : Effective Young's modulus of cellular materials
E : Young's modulus of solid material
G^* : Effective shear modulus of cellular materials
G : Shear modulus of solid material
h, l : Cell wall lengths of cellular materials
I(x) : Second moment of area of cell walls
k : Shear correction coefficient
M_h : Axial compliance of the cell wall with length h
M_l : Axial compliance of the cell wall with length l
N_h : Bending compliance of the cell wall with length h
N_l : Bending compliance of the cell wall with length l
ν^* : Effective Poisson ratio of cellular materials
ν : Poisson ratio of solid material
ρ^*_M : Relative density of cellular materials
σ_e : Von-Mises stress on the surfaces of non-uniform struts

References

[1] L. J. Gibson, M. F. Ashby, G. S. Schajer and C. I. Robertson, The mechanics of two-dimensional cellular materials, *Proceedings of the Royal Society of London*, A382 (1982) 2542.

[2] C. M. Ford and L. J. Gibson, Uniaxial strength asymmetry in cellular materials: An analytical model, *International Journal of Mechanical Sciences*, 40 (1988) 521-531.

[3] J. W. Klintworth and W. J. Stronge, Elasto-plastic yield limits and deformation laws for transversely crushed honeycombs, *Journal of Mechanical Sciences*, 30 (1988) 273-292.

[4] L. J. Gibson, M. F. Ashby and J. Zhang, Triantafillou TC. Failure surfaces for cellular materials under multiaxial loads. I. Modelling, *International Journal of Mechanical Sciences*, 31 (1989) 635-663.

[5] L. J. Gibson and M. F. Ashby, Cellular materials: structure & properties, Cambridge University Press, Cambridge, (1997).

[6] W. E. Warren and A. M. Kraynik, Foam mechanics: The linear elastic response of two-dimensional spatially periodic cellular materials, *Mechanical Materials*, 6 (1987) 2737.

[7] W. E. Warren and A. M. Kraynik, The linear elastic properties of opencell foams, *Journal of Applied Mechanics*, 55 (1988) 341-346.

[8] T. C. Triantafillou, J. Zhang, T. L. Shercliff, L. J. Gibson and M. F. Ashby, Failure surfaces for cellular materials under multiaxial loads. II. Comparison of models with experiments., *International Journal of mechanical Sciences,* 31 (1989) 665-678.

[9] M. J. Silva, W. C. Hayes and L. J. Gibson, The effect of non-periodic microstructure on the elastic properties of two-dimensional cellular solids., *International Journal of mechanical Sciences*, 37 (1995) 1161.

[10] A. M. Kraynik, M. K. Neilsen, D. A. Reinelt and W. E. Warren, Foam micromechanics, *In: Proceedings of the NATO Advanced Study Institute on Foams, Emulsions and Cellular Materials*, Cargese (1997) Corsica.

[11] J. L. Grenestedt, Influence of wavy imperfections in cell walls on elastic stiffness of cellular solids, *Journal of Mechanics and Physics of Solids*, 46 (1998) 29.

[12] A. E. Simone and L. J. Gibson, Effects of solid distribution on the stiffness and strength of metallic foams, *Acta Mater*, 46 (1998) 2139-2150.

[13] C. Chen, T. J. Lu and N. A. Fleck, Effect of imperfections on the yielding of two-dimensional foams, *Journal of Mechanics and Physics of Solids*, 47 (1999) 2235-2272.

[14] V. S. Deshpande and N. A. Fleck, Isotropic constitutive models for metallic foams, *Journal of Mechanics and Physics of Solids*, 48 (2000) 1253-1283.

[15] H. S. Kim and S. T. S. Al-Hassani, A morphological elastic model of general hexagonal columnar structures., *International Journal of mechanical Sciences*, 43 (2001) 1027-1060.

[16] J. S. Huang and T. W. Chen, Survival probability for brittle honeycombs with plateau borders under uniaxial compression, *Acta Mechanica*, 164 (2003) 61-74.

[17] H. S. Kim and S. T. S. Al-Hassani, Plastic collapse of cellular structures comprised of doubly tapered struts, *International Journal of mechanical Sciences*, 43 (2001) 2453-2478.

[18] H. S. Kim and S. T. S. Al-Hassani, The effect of doubly tapered strut morphology on the plastic yield surface of cellular materials, *International Journal of Mechanical Sciences*, 44 (2002) 1559-81.

[19] J. M. Gere and S. P. Timoshenko, Mechanics of materials, Chapman & Hall, London, (1991).

[20] H. S. Kim and S. T. S. Al-Hassani, Effective elastic constants of two-dimensional cellular materials with deep and thick cell walls, *International Journal of Mechanical Sciences*, 45 (2004) 1999-2016.

[21] H. S. Kim and S. T. S. Al-Hassani, Effective elastic constants of two-dimensional cellular materials with deep and thick cell walls, *International Journal of Mechanical Sciences*, 45 (2003) 1999-2016.